GENERAL AND APPLIED PHYSICS

Analysis Structural Modification and Optical–Electrical Properties of Al-Doped ZnO Oxide Films Deposited by Magnetron Sputtering

E. J. C. Santos[1] · J. C. A. Queiroz[2] · M. G. O. Queiroz[3] · M. S. Liborio[4] · E. O. Almeida[2] · K. L. Bessa[2] · R. R. M. Souza[5] · M. C. Feitor[2] · T. H. C. Costa[2]

Abstract

This study aims to assess structural, optical, and electrical properties of AZO thin films produced by magnetron sputtering in high pressure were 12, 7, and 5 cm apart between the target and the glass substrate. Then, a treatment current variation (0.1, 0.2, and 0.3 A) was performed for the fixed position of 5.0 cm away. Characterization techniques such as XRD, SEM, and EDS were used to investigate the structural changes and composition of the deposited films. Besides, spectrophotometry enabled an analysis of the optical constants, and the four-point probe assay was used to measure the film electrical resistance. The results showed that the approximation between the target/substrate, and the increase in current from 0.1 to 0.3 A, produces an increase in crystallinity, grain size, and film thickness. These factors promote a reduction in transmittance, bandgap energy, and electrical resistivity. Sample A503 (5.0 cm and 0.3 A) showed the best electrical properties (2.18 x 10^1 Ω.cm) in view of the set of parameters adopted in this work.

1 Introduction

Producing new materials through processes where the conditions of synthesis and growth determine factors for the applications performance represents a significant challenge for researchers who try to make materials with specific physical and chemical properties viable from changes in their microstructure [1–9].

The interest in thin films was due to the industry advances in new technologies based on nanomaterials that resulted in a series of applications to improve people daily lives. In this way, the application of thin films extends to optical-electronic devices [10], functional coatings [11],and in the generation and conservation of energy [12]. Thin transparent conductive oxide films (TCOs) are presented as alternatives

✉ J. C. A. Queiroz
 cesar.augusto.049@ufrn.edu.br

 E. J. C. Santos
 edjosecosta@hotmail.com

 M. G. O. Queiroz
 mariagerlania@hotmail.com

 M. S. Liborio
 maxwellsantana@ect.ufrn.br

 E. O. Almeida
 edalmy@gmail.com

 K. L. Bessa
 fis777@ufrn.edu.br

 R. R. M. Souza
 romulorms@gmail.com

 M. C. Feitor
 mcfeitor@gmail.com

 T. H. C. Costa
 thercioc@gmail.com

1 Federal Institute of Technological Education, Currais Novos, Brazil

2 Department of Mechanical Engineering, Federal University of Rio Grande do Norte, Natal, Brazil

3 Federal Rural University of the Semi-arid, Paus dos Ferros, RN, Brazil

4 School of Science and Technology, Federal University of Rio Grande do Norte, Natal, Brazil

5 Department of Mechanical Engineering, Federal University of Piauí, Natal, Brazil

that can meet specific demands depending on their electrical nature. It can present conductivity of type *p* or *n*, depending on the dopant chosen to incorporate the TCO lattice [13]. The performance of devices with thin films TCOs as their operating principle depends on their electrical and optical properties.

Among the TCOs materials obtained in thin films, tin-doped indium oxide (ITO) is the most favorable for high-performance applications due to the balance between electrical and optical properties [14]. However, the use of ITO is limited due to the scarcity, high price, and toxicity of the Indian [15–17]. The emerging and growing demand for TCO films of low economic value and high performance is the fuel that drives research that aims to investigate how the electrical and optical properties of these films can be obtained in an optimized and increasingly accessible way [18–20].

In this scenario, doped zinc oxide thin films appear promising candidates for TCO applications [21–23]. With an emphasis on ZnO doped with aluminum (AZO), which, due to its balance between optical and electrical properties, attracted researchers attention as a potential substitute for ITO. AZO has desirable properties, such as long-term environmental stability [24], high optical transmittance in the visible region [25], high electrical conductivity [26], non-toxicity [27], abundance, and low cost [28]. Regarding the bandwidth, the desired value of the energy gap for a thin TCO film should be relatively high, that is, above 3.2 eV. This value allows most of the light in the solar spectrum to pass through the TCO films microstructure, preventing it from being absorbed [29].

Although AZO thin films have this range of advantages, their electrical and optical properties remain inferior in terms of performance when compared to ITO films [30]. Therefore, how to provide the best conditions for depositing a high-quality AZO film becomes an issue of high relevance in TCO applications.

Several studies indicate AZO films with high crystallinity obtained from deposition processes with high temperatures in the literature about TCO thin films. But unfortunately, this increase in temperature compromises the optical properties, making the films from this process slightly opaque [31, 32]. In this scenario, many researchers believe that producing a film with a periodic crystalline structure at a relatively low process temperature is the key to preparing thin, highly conductive, and transparent AZO films [33]. According to Şenay (2019), optimizing deposition parameters, such as spray power, pressure, and distance from the target substrate, allows obtaining high-quality films [34]. According to the author, previous research [35–38] related to the good combination of film deposition parameters also argues that the thickness of the AZO films layer could have a significant influence on their properties.

This work investigates the influence of deposition parameters: target–substrate distance and electric spray current, in the synthesis of thin films of AZO obtained by magnetron sputtering without annealing and at high pressure on a glass substrate. The variation of these parameters is related to the structural and physical properties of AZO films to investigate the best combination between variation in distance and electric current value in the deposition. Therefore, the purpose of this research is to produce AZO thin films with good quality, suggesting acceptable deposition parameters and thus raising AZO films to the level of an alternative to ITO thin films for existing applications.

2 Materials and Methods

AZO films were deposited on glass substrates with dimensions of 25 mm x 15 mm and a thickness of approximately 1.0 mm. Before the deposition process, the substrates were cleaned in an ultrasonic bath with distilled water, ethanol, and acetone, respectively, for 10 min and then dried with an air jet. For the formation of AZO thin films, a magnetron sputtering deposition system with direct current (DC) was used in details given previous report [28]. A commercial ceramic target with a chemical composition of Al_2O_3 and ZnO, with an atomic weight ratio equal to 98:2% and purity content of approximately 99.95%, was used as a precursor material source for film synthesis. The target is 6.30 mm thick and 50.0 mm in diameter. In this study, the distance between the target and the substrate, as well as the electric current, varied. These parameters were responsible for structural changes and variations in AZO thin films final optical and electrical properties. Table 1 shows the detailed conditions for sputtering.

The analysis of the crystalline phases of the AZO films, the BRUKER X-Ray diffractometer (model D2 PHASER) with an angle of 0.02 ° was used. The average crystallite size (τ) was determined by the Scherrer equation [39]. The films surface was characterized using a ZEISS AURIGA 40 Scanning Electron Microscope with X-ray Dispersive Energy (EDS) spectra coupled to the FEG for semi-quantitative analysis of the chemical composition. For morphology analysis,

Table 1 Magnetron sputtering deposition parameters

Samples	Argon flow (cm²/min)	Pressure (mBar)	Time (min)	Distance (cm)	Electric current (A)
A501					0.1
A502				5.0	0.2
A503	20	1.0×10^{-1}	30		0.3
A703				7.0	0.3
A1203				12.0	0.3

a Shimadzu atomic force microscope, model SPM-9700, was used, using the Modular Force method with constant force and a resonance frequency of 75 kHz. The films optical transmittance spectra were performed by the spectrophotometer Genesys 10uv from the Thermo Fisher Scientific brand. From the values of the percentage of radiation transmission in the AZO film structure, the bandgap energy was determined using the Tauc relationship [40]. Electrical resistivity measurements were performed using the four-point method described by Chandra et al. (2011) [41].

3 Results and Discussion

3.1 Variation of the Target-Substrate Distance

Figure 1 shows the AZO ceramic target diffractograms and the thin AZO films deposited on a glass substrate, corresponding to the target-substrate distances equal to 5.0, 7.0, and 12.0 cm. And Fig. 1b shows the same XRD patterns, emphasizing the diffraction peak (002), showing a displacement as a function of the variation of target-substrate distance.

According to Zhao et al. (2021), considering the target as a solid tablet with a defined stoichiometric relationship of ZnO:Al, sample synthesis with nucleation of crystallographic planes similar to that of the target was already expected [15].

The targets XRD pattern confirms that it has a compact hexagonal structure, with a total absence of crystallographic phases referring to Al or Al_2O_3, indicating that the process of replacing the Zn atoms by Al occurs effectively [8]. All diffraction peaks are perfectly indexed to the ZnO wurtzite phase: $2\theta = 31.50°$ (100), 34.07° (002), 35.92° (101), 47.22° (102), 56.33° (110), 62.44° (103), 66.11° (103) and 67.47° (200), with lattice constants $a = 3.2545$ Å and $c = 5.2056$ Å, according to Inorganic Crystal Structure Database (ICSD) crystallographic chart N° 67848. All films showed diffraction peaks referring to the ZnO phases, showing a growth of planes with orientation along the c axis, direction [0001], and perpendicular to the substrate surface [16]. According to Fujimura et al. (1993), the nucleation of grains along the c axis, on the surface of amorphous substrates, is related to the lower free energy for forming a crystallographic plane. Besides, the surface diffusion promotes the preferential orientation of the nuclei towards the crystallographic direction with less surface energy, which corresponds to the plane (002) [42].

The variation of target-substrate distance resulted in the formation of films with different crystallinity. A change in peak intensity and the appearance of characteristic phases of the planes (100), (101), and (110) indicated the growth of a film thin with a similar structure to the AZO target (ZnO:Al). This similarity observed in the atomic structure of the films in relation to the target becomes more evident as the distance between the surface of the substrate and the
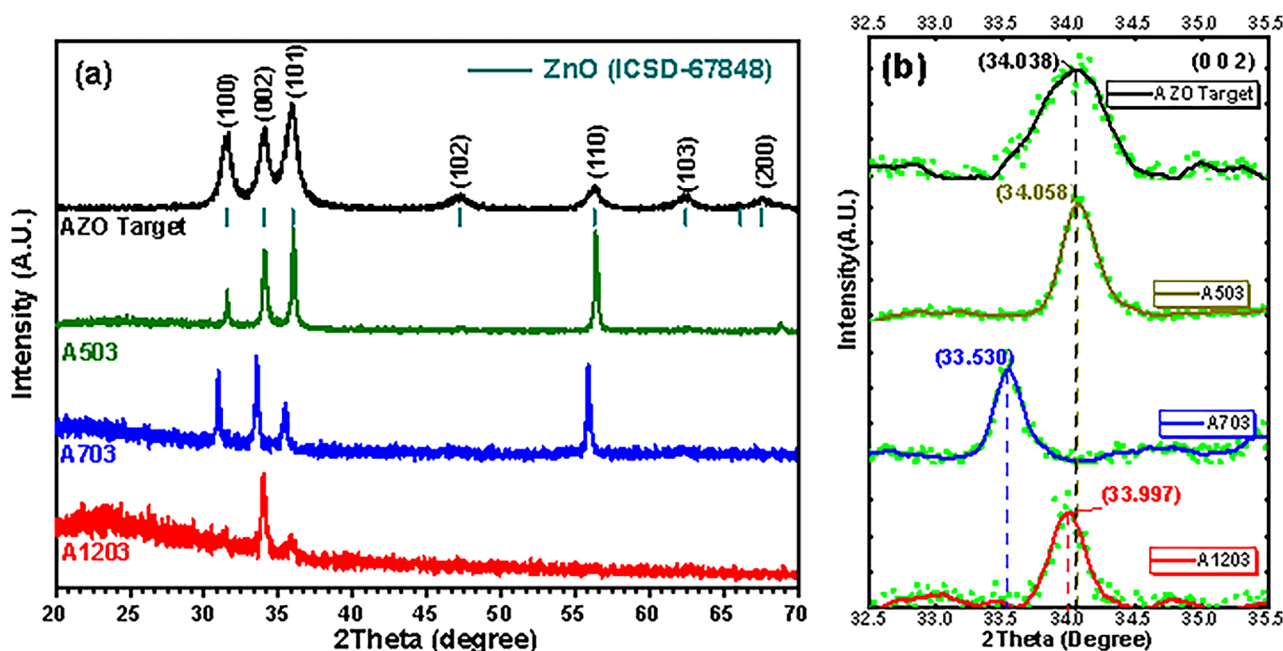

Fig. 1 Diffractogram of AZO thin films deposited by magnetron sputtering with a variation of target-substrate distance: (**a**) complete XRD, and (**b**) peak magnification (002)

target decreases, causing an increase in temperature during the deposition process, which is a fundamental factor for the modification structure of films deposited by sputtering [43].

The diffraction peak (002) of AZO thin films has its position changed to values 2θ higher or lower concerning pure ZnO [38]. When Al is incorporated into the ZnO lattice, the AZO lattice distorts due to the difference between the radius of the Al^{3+} (0.54 Å) and Zn^{2+} (0.74 Å) [44]. Suppose the Al^{3+} ions only replace the Zn^{2+} ions. In that case, the lattice parameters (*a* and *c*) of the ZnO crystal decrease, also causing the interplanar distance *d* (hlk) to be reduced, and the peak position (002) changes to high values of 2θ, according to the Bragg law [45]. This displacement was observed for the sample A503 (see Fig. 1b), characterizing a small accumulation of stresses produced by Zincs substitution for aluminum in the ZnO:Al lattice during plasma deposition [36]. On the other hand, in the diffractograms of the samples positioned at 12 cm (Al_2O_3) and 7 cm (A703), a peak displacement (002) for lower angles is noted. This change results from residual tensile stresses that increased the lattice parameters due to the change in the chemical bonds length. That indicates that Al^{3+} also occupied interstitial sites, as reported in other studies [18–20, 45].

The crystallite size of AZO films was evaluated as a function of the target substrate distance from the peak FWHM (002) of the XRD standard using Scherrer formula [46]. Figure 2 shows that the reduction of the target-substrate distance from 12 to 7 cm caused a considerable increase in the crystallite size, which is one of the most important influences on AZO films conductivity. This effect was produced by the aluminum doping content (Table 2). When the content of Al in ZnO increases, the FWHM of the peak (002) becomes larger, indicating that the crystallite size of thin films of Al:ZnO decreases with the increase in the content of Al in the films. This result is consistent with other measurements

Table 2 Thickness and composition of AZO thin films deposited by magnetron sputtering

Samples	Thickness(nm)	Composition (at. %)		
		Zn	O	Al
A503	1180 ± 36.0	51.27	46.58	2.15
A703	1052 ± 23.1	47.53	50.62	1.85
A1203	446 ± 38.3	31.66	49.16	2.46

[47, 48]. According to Lee et al. (2021), the deterioration of the films crystallinity caused by excess aluminum doping is caused by residual tensions [49].

According to Gopikishan et al. (2017), the variation in temperature and electron density in the target surface axial direction are reported [50]. The confinement of secondary electrons increases ionization efficiency, which is the cause of high density and temperature in front of the target, which results in the rapid growth of nanoparticles [51]. However, the small variation in distance from 7 to 5 cm caused a reduction in the size of the crystallite, indicating an increase in the grain boundary region [52], as well as a slight increase in temperature, which on the other hand, allowed a slight increase in deposition rate. The crystallite size can influence the concentration of charge carriers on the surface of the film, changing the nature of the energy barrier, favoring electrical mobility, that is, making the film a better semiconductor [53].

Table 2 shows the chemical composition of AZO films performed by EDS on the surface of the samples. The compositions obtained are in accordance with the results described by Ghobadi et al. (2021), where it presents an oxygen content of approximately 50% [54]. It can be seen in the EDS results that the Zn content gradually decreases as a function of the distance. This fact is due to the reduction of

Fig. 2 Variation of FWHM, crystallite size, and deposition rate as a function of the sample distance from the target in magnetron sputtering deposition
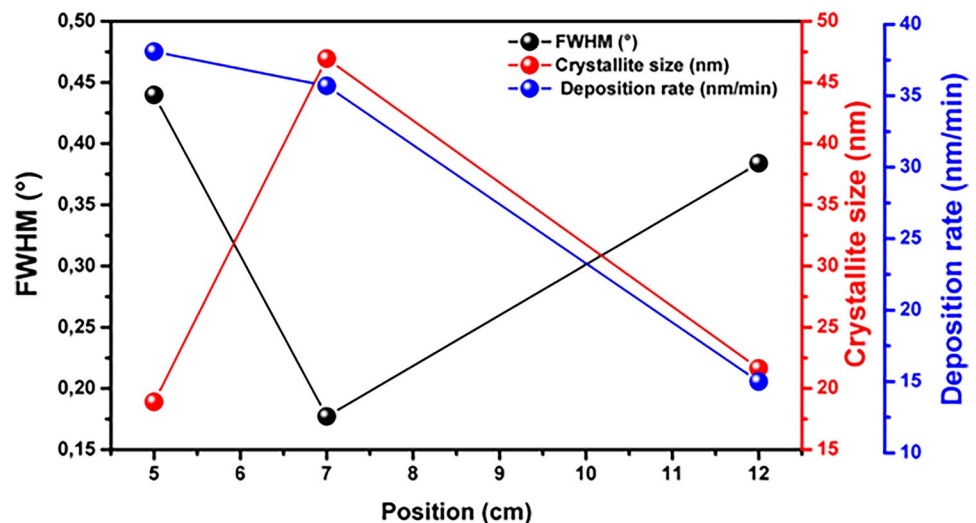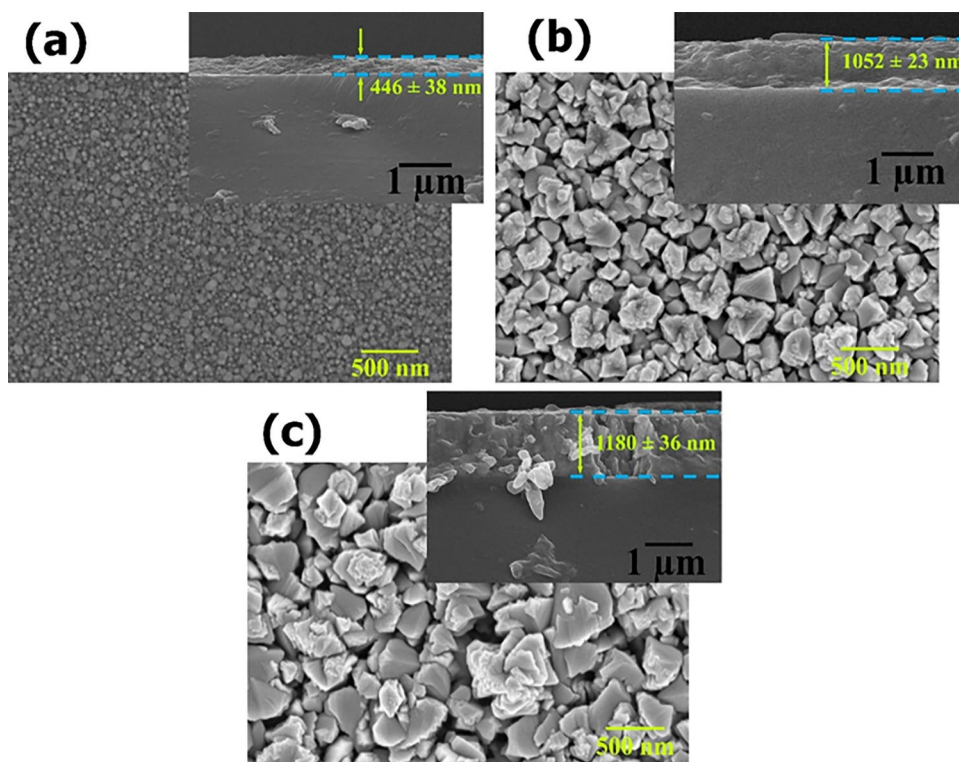
Fig. 3 Superficial micrograph of AZO films deposited with distances of (**a**) 12.0, (**b**) 7.0, and (**c**) 5.0 cm concerning the target (Images at 10kX and 50kX magnification)

the film thickness caused by the sample positioning concerning the AZO target.

Figure 3 presents the electron microscopy images of the cross-section and surface of the thin films of the AZO.

The films are homogeneous and have adequately adhered to the substrate. The grains shown are domains formed by the aggregation of crystallites on a nanometric scale. It is found that the grain size of AZO films increases as the distance to the substrate decreases due to the increased thickness of the deposited film. That is probably because, at shorter distances, the rate of deposition of atoms is higher, causing greater nucleation density and greater diffusion on the surface [52]. Therefore, more elongated grains are produced by the coalescence of neighboring grains on the substrates closest to the target [43]. The oriented cores (002), predominant in sample Al_2O_3, grow perpendicularly to the substrate surface; on the other hand, the oriented cores (100), (101), and (110), more intense in samples A703 and A503 (see Fig. 1), have other orientations. Therefore, target-substrate approximation resulted in morphological changes caused by nucleation and grain formation with different crystallographic orientations.

The average optical transmission of the films obtained with different target-substrate distances is shown in Fig. 4. The transmittance spectrum in the visible range (380-780 nm) of sample Al_2O_3 showed values around 80%. In comparison, sample A703 showed values above 70% between 550 nm and 780 nm, which are important for applications such as radiation filters and even solar cells [55].

On the other hand, sample A503 presented a low percentage of optical transmittance in the visible range, presenting an optical response similar to an opaque material [56]. It was found that the reduction of the target-substrate distance influenced the optical transmittance of the films. Such reduction is related to the increase in temperature, the compression of the crystalline planes by diffusion of the deposited atoms, and, consequently, the greater thickness of the film
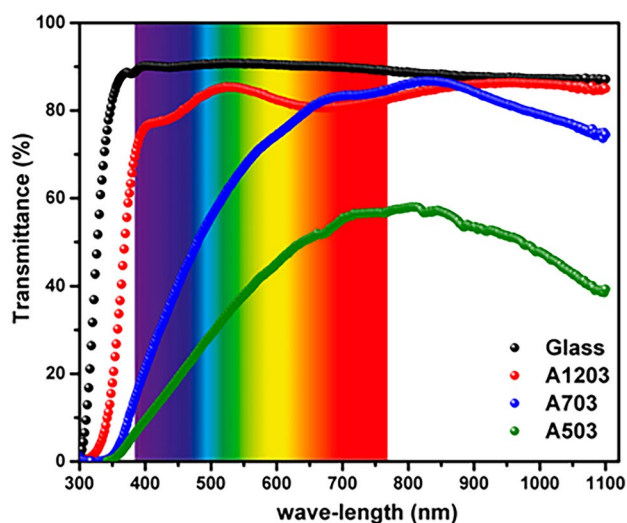

Fig. 4 Optical transmittance of AZO thin films obtained by magnetron sputtering with different target-substrate distances
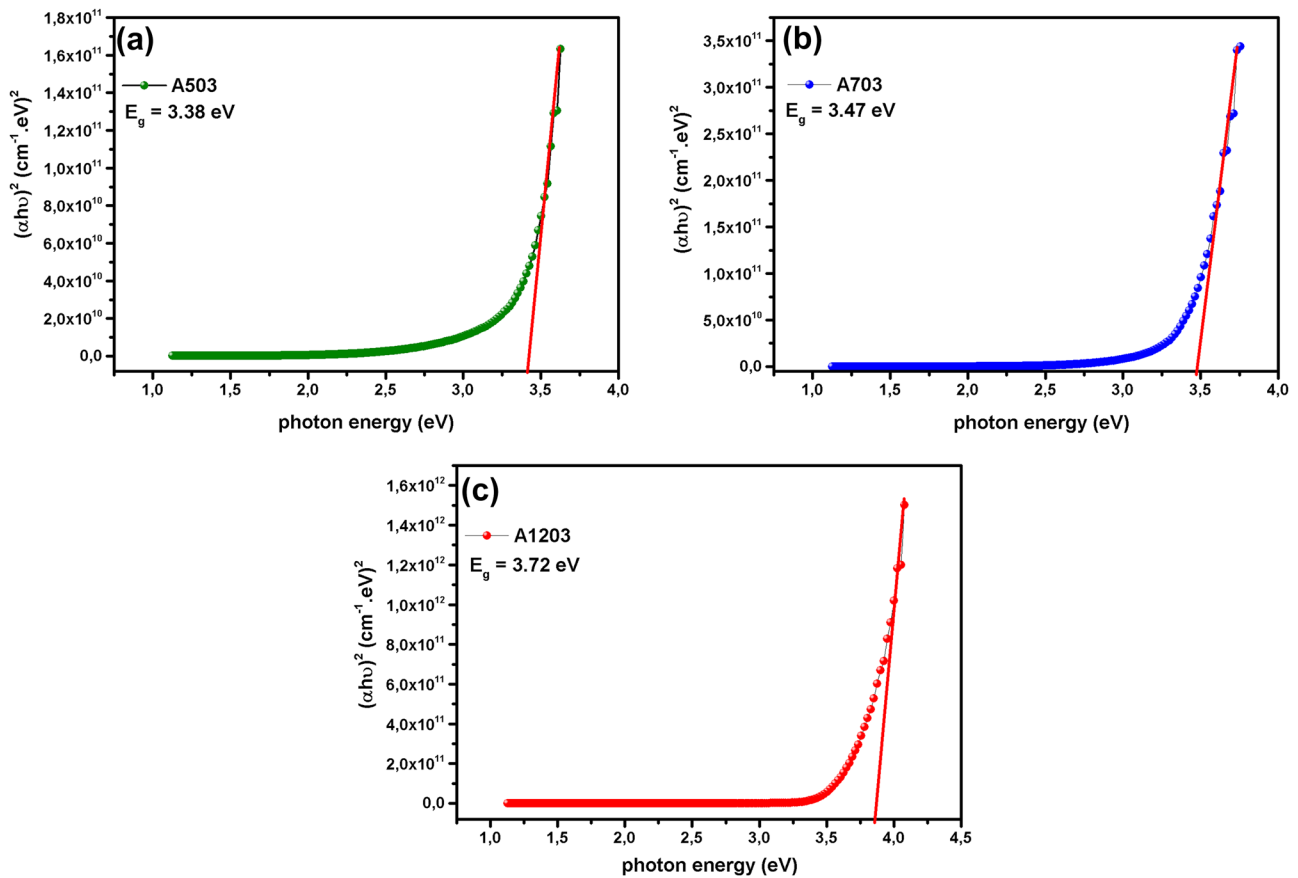
Fig. 5 Curve $(\alpha h\nu)^2$ versus photon energy for AZO films for different distances: (**a**) 5 cm, (**b**) 7 cm, and (**c**) 12 cm

that causes the free absorption of the carrier, which increases the concentration of the carrier in the thick film and leads to the absorption of more light [57].

But according to Dejam et al. (2016), the reduction in the percentage of transmittance can also be related to the high content of Zn in the chemical composition of the film, since the chemical species of Zn^{2+} absorb a vast number of wavelengths, allowing the film to behave similarly to metal [58]. Thus, the low transmission of the A503 film can be justified by Zn high presence, as shown in Table 2. The spectra absorption edge characterized by the sharp drop in transmittance was observed in the range between 300 and 400 nm. It can be seen in Fig. 2 that the absorption edge changes to shorter wavelengths as the target-substrate distance increases. According to Turkoglu et al. (2018), this change can be attributed to an increase in the bandgap energy resulting from the Brustein-Moss effect, which is related to the concentration of carriers [59]. With the increase of the target-substrate distance, the films gap energy increases due to the increase of the carrier concentration and causes the absorption edge to change to short wavelengths.

The study of the optical properties of the AZO films analyzed is of particular interest. It allows us to determine other parameters. The bandgap is hugely relevant for indicating the type of electronic transition between the energy bands [60]. Figure 5 shows the curve with bandgap energy values $(\alpha h\nu)^2$ versus photon energy for AZO films produced with different distances. Considering the ZnO doped with Al a direct gap material, the experimental values of optical absorption were measured considering n = 2. We can conclude that the electronic transitions are of the direct type. The energy band interval values decreased from 3.72 to 3.38 eV when the distance decreased from 12.0 to 5.0 cm.

That is due to the better crystallinity of the structure presented by the films through the target-substrate approach. This change in structure makes the electrical behavior of

Table 3 Values of deposition rate and electrical resistivity for AZO films

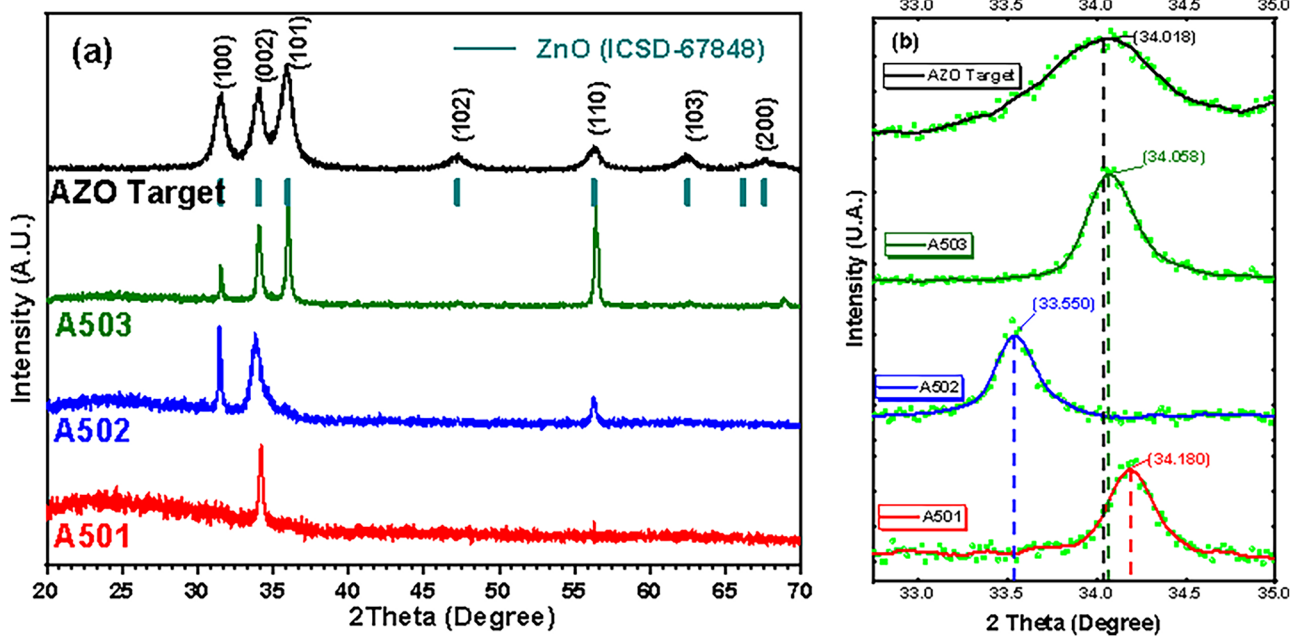| Samples	Discance (cm)	Electrical resistivity (Ω.cm)
A503	5	2.18×10^1
A703	7	4.2×10^2
A1203	12	5.86×10^5

Fig. 6 XRD spectra of AZO films deposited with an electric current variation

the film closer to that of semiconductor materials. The optical gap energy of ZnO is approximately 3.34 eV, and the increase in E_g values obtained in this work is due to the Burstein-Moss effect, which is the increase in the Fermi level in the semiconductor conduction band due to the increase in carriers caused by doping with aluminum [38, 61].

Table 3 shows the electrical resistivity values of AZO films without annealing, obtained with different positions. The results showed that the shortest target-substrate distance produced the most conductive film. That effect is associated with the reduction of the gap energy for this treatment condition. Sample A503 showed higher crystallinity and larger grain size. Therefore, the dispersion of the grain limit and

the increase in the load carriers life led to a decrease in resistivity, according to experimental results by Jang et al. (2021) [62].

3.2 Electric Current Variation

The thin films of AZO produced with variation in distance between the target and the sample holder showed that the film A503 (with 5.0 cm of distance) showed the best result for electrical conductivity. Therefore, the electric current was varied with the fixed distance at this value.

Figure 6 shows the XRD spectra of AZO films obtained with electrical current values of 0.1, 0.2, and 0.3 A. The

Fig. 7 Variation of FWHM, crystallite size, and deposition rate as a function of the electric current in the deposition process
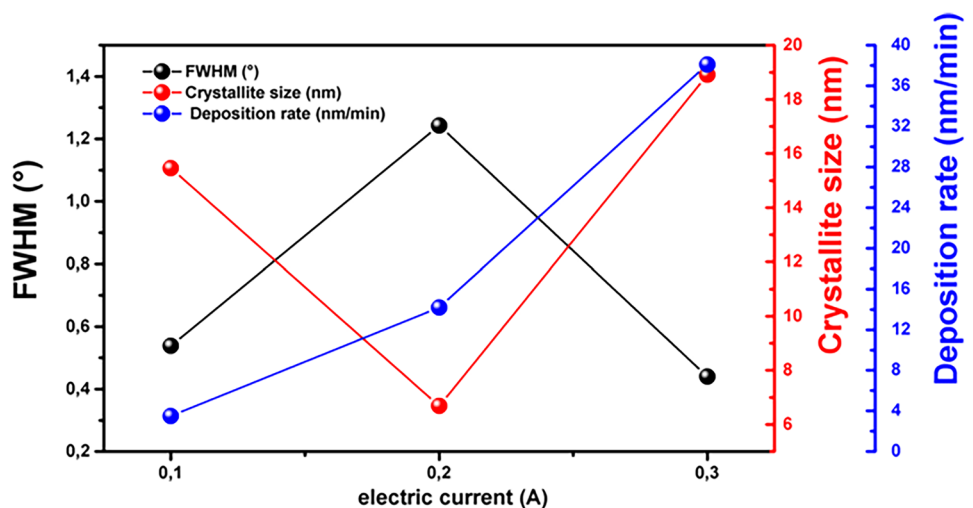
Table 4 Thickness and Composition of AZO thin films deposited by magnetron sputtering with an electric current variation

Samples	Thickness(nm)	Composition (at. %)		
		Zn	O	Al
A503	1180 ± 36.0	51.27	46.58	2.15
A502	426 ± 16.9	44.00	53.54	2.46
A501	315 ± 23.8	11.81	85.08	3.11

diffraction result obtained from the films analysis produced at 0.1 A (A501) shows the formation of a mono film-crystalline and preferential plan orientation (002). In this case, the low electric current provides insufficient kinetic energy for the nucleation process of more stable crystallographic planes. This is the factor responsible for the emergence of residual compression stresses and, consequently, a displacement from the peak to the right. On the other hand, greater deformation energy will be promoted in the films because of the moment transfer caused by the bombardment of ions, resulting in the development of different crystallographic orientations observed in the diffractograms of the films produced with greater electrical current (A502 and A503).

Figure 6 shows that the increase in electrical current from 0.1 to 0.3 A makes the thin film structure deposited more crystalline and similar to the structure of the target. This similarity stems from the dimensional stability of the planes formed due to the higher processing temperature. Besides,

the formation of a tail on the right side of the peak (002) of the A502 sample is noted. This asymmetry results from the excess of aluminum in the film composition, causing high distortion in the lattice [63].

Figure 7 shows the variation in crystallite size resulting from the increase in electrical current. The reduction of this sample A502 was unexpected since the increase in temperature caused by the electric current allows for more stable crystallographic planes with less binding energy.

The composition of AZO films deposited with an electric current of 0.2 and 0.3 A showed Zn and O balance similar to the results obtained for films produced with 7 and 5 cm of target-substrate distance (samples A703 and A503). On the other hand, as observed in sample Al_2O_3, the composition of the A501 film showed a significant imbalance regarding the values of Zn and O in the AZO thin film (Table 4). The low sputtering energy can explain this result concerning the binding energy of the cathodic targets surface, which results in lower spray performance. In this case, only atoms that are weakly bound to the surface or species adsorbed in the targets manufacturing process are more easily ejected [64]. AZO films with high oxygen content and low zinc content, as presented in samples A501 and Al_2O_3, are unfavorable for application as conductive oxides [51].

Figure 8 shows the transverse and surface microscopy images of the AZO films produced with an electric current variation. The films remained homogeneous and adhered to the substrate. The surface images show the increase in

Fig. 8 Superficial micrograph of AZO films deposited an electric current variation of (**a**) 0.1 (magnifications of 8.0 kX and 50 kX), (**b**) 0.2 (magnifications of 10.0 kX and 50 kX), and (**c**) 0.3 cm (magnifications of 10.0 kX and 50 kX)
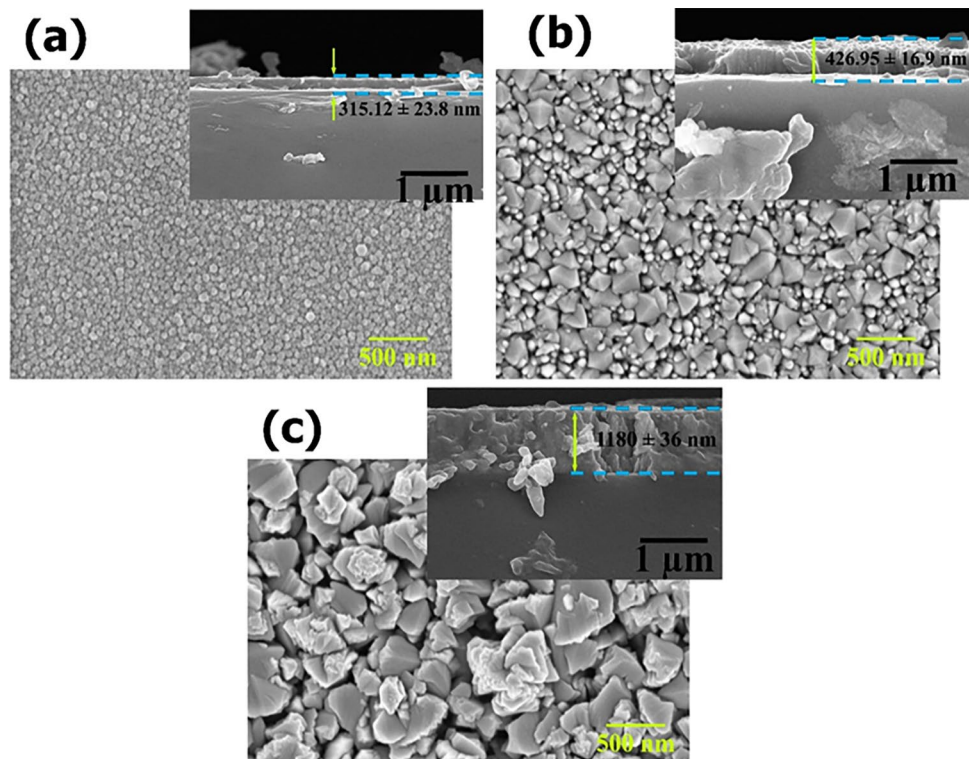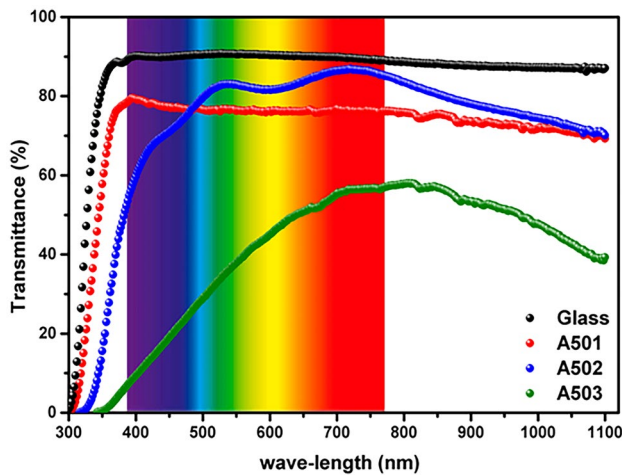
Fig. 9 Optical transmittance of AZO thin films obtained by magnetron sputtering with different electric current values

grain size as a function of the increase in electrical current. According to Barman et al. (2021), high values of power (and consequently greater electrical current) cause an increase in the kinetic energy with which the ZnO particles reach the substrate, resulting in morphological differences in the deposited films [65]. This effect favors the formation of denser and more compact films, these characteristics being favorable to optical and electrical properties. The increase in electrical current increased the substrate temperature and obtaining AZO films with larger grain sizes. Studies show that the decrease in temperature results in a reduction in grain size due to low diffusion energy, making it difficult to reorganize atoms and leads to the formation of small crystallites [66, 67]. Comparing the SEM-FEG images and the XRD spectra of the AZO films, it is possible to verify that the best crystallographic properties are found for larger grains. According to Yujin et al. (2021), the increase in grain size generally leads to a smaller contribution of grain contours to load carriers spread [68].
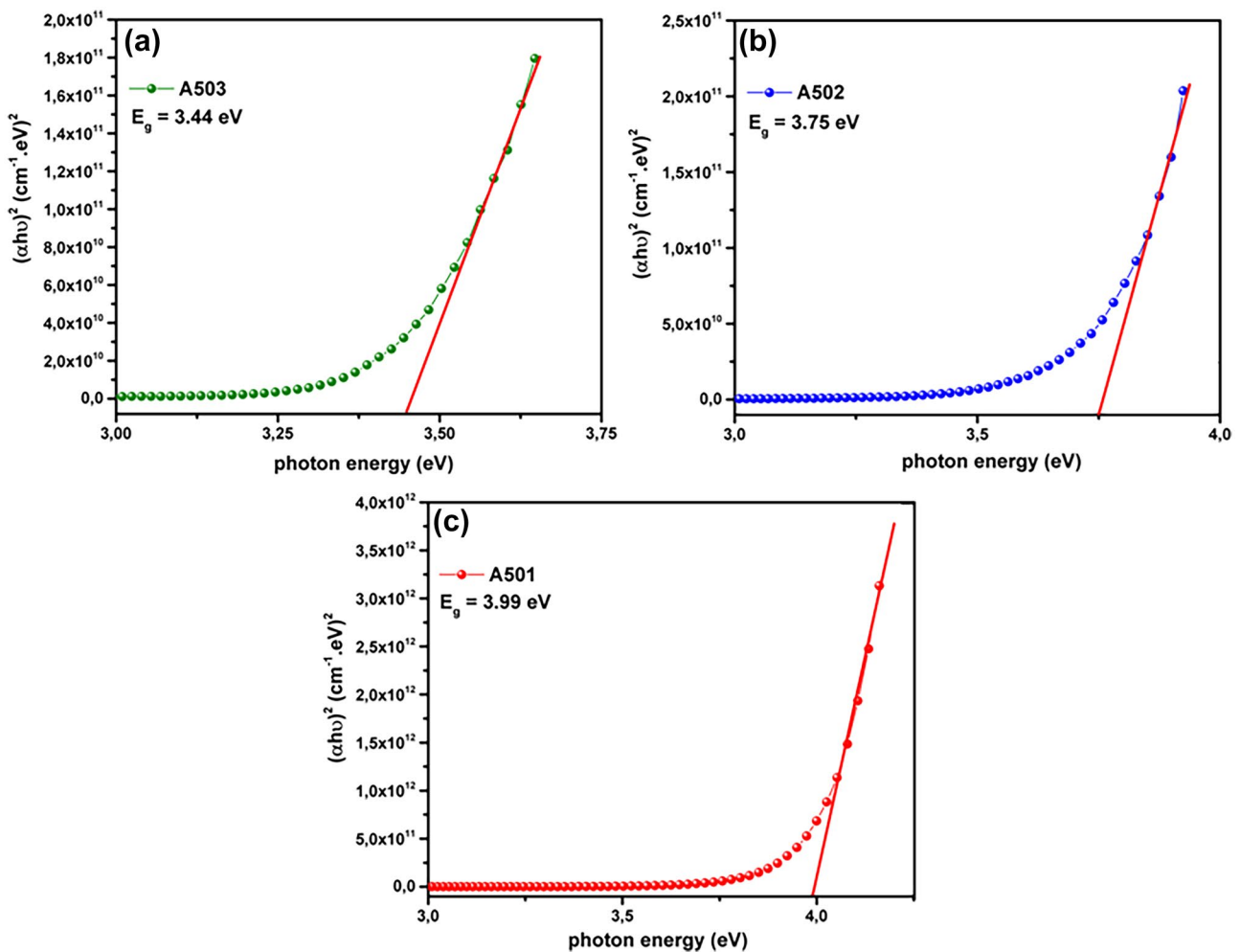

Fig. 10 Curve $(\alpha h\nu)^2$ versus photon energy for AZO films for different electrical current: (**a**) 0.3 A, (**b**) 0.2 A, and (**c**) 0.3 A

As a result, larger grains favor the increase in electrical conductivity. Figure 8b shows several smaller spherical structures, indicating grains growth by aggregating several crystallites (clusters). This fact is reported in the literature and is caused mainly by high surface energies, characteristics of films deposited with high thicknesses, and powers [69, 70]. The SEM-FEG image of the AZO films surface obtained without annealing in this work with 0.1 A shows a morphology similar to the AZO films obtained by Vasile et al. (2021) after annealing at 300 °C and 500 °C. This shows the methods efficiency and the choice of parameter sets adopted in this work to obtain AZO films without annealing [71]. Therefore, the annealing step to improve the films properties becomes unnecessary, given the choice of parameters adopted in the present study.

The average optical transmission of the films obtained with different electrical currents is shown in Fig. 9. The transmittance spectrum in the visible range (400-800 nm) of the A502 sample obtained with 0.2 A electrical current showed transmittance above 80%.

The sample A501 showed values above 70%, making it optically good candidates for photovoltaic applications. However, the A503 sample showed low transmittance in the visible spectrum with a maximum value of close to 60%. The increase in the electric current provided an increase in the films deposition rate and a decrease in optical transmittance. That result may be associated with Zn amount in the AZO film that also increases with the electric current, as shown in the EDS analysis (Table 4). Besides, the transmittance decreases due to the increase in temperature during the growth of AZO films, causing an increase in defects on the films surface, as observed in the SEM surface of the A503 samples (Fig. 8).

Figure 10 shows the curve $(\alpha h\nu)^2$ versus photon energy for AZO films for different electrical currents. The optical gap energy range value decreases from 3.99 eV to 3.44 eV when the electric current increases from 0.1 A to 0.3 A. The gap energy shift is associated with the Burstein-Moss effect. Sun et al. (2016) and Challali et al. (2020) found similar behavior between RF power and gap energy values in which

the decrease in the gap due to the increase in power resulted in a reduction in the concentration of cargo carriers [63, 71].

Table 5 shows the variation in the electrical resistivity of AZO films for electrical currents from 0.1 to 0.3 A. With the increase in electrical current, a decrease in resistivity of 10^3 the value obtained with an electrical current of 0.1 A. occurred. Observed in the analysis for different target-substrate distances, the increase in the crystallinity of the AZO thin film, the consequent increase in the grain size, and the reduction of the bandgap energy due to the increase in current characterizes a better result in terms of electrical conductivity.

4 Conclusion

This work reports the results obtained through magnetron sputtering deposition of AZO thin films without annealing and high pressure on the glass. The variation of target-substrate distance and current sputtering was adopted to evaluate these parameters influence on the structural, optical, and electrical properties of the films. The XRD spectra for different target-substrate distances and electric current showed the formation of films with different crystallinity. However, thin films have a similar structure to that of the AZO target (ZnO:Al) as the target-substrate distance decreased and the electric current increases. The results of SEM-FEG showed that the films were deposited homogeneously and appropriately adhered to the substrate. However, the film deposited at 5.0 cm of target-substrate distance and an electrical current of 0.3 A showed a high deposition rate due to the high ionic bombardment on the substrate, and consequently, greater thickness. However, this thickness caused a drastic reduction in the transmission of radiation in the visible range.

Combining the effects resulting from this treatment configuration (high pressure, target-substrate distance, and electric current) produced thin AZO films with different characteristics. However, sample A503 showed higher crystallinity, larger grain size, and gap energy closer to pure ZnO (3.44 eV). This treatment configurations resulting and conclusive effect was a significant reduction in electrical resistivity, making the AZO thin film about 10^4 times more conductive without subsequent annealing (2.18×10^1 Ω.cm).

Table 5 Values of deposition rate and electrical resistivity for AZO films

Samples	Electric current (A)	Electrical resistivity (Ω.cm)
A503	0.3	2.18×10^1
A502	0.2	1.70×10^3
A501	0.1	3.29×10^4

References

1. A. Hamidi, E. Mahboub, K. Meziane, A. Hichou, A. Almaggoussi, Optik. (2021). https://doi.org/10.1016/j.ijleo.2021.167070

2. J.M. Ribeiro, F.C. Correia, P.B. Salvador, L. Rebouta, L.C. Alves, E. Alves, N.P. Barradas, A. Mendes, C.J. Tavaresa, Vacuum (2019). https://doi.org/10.1016/j.vacuum.2018.12.038

3. A.T.T. Pham, P.A.T. Nguyen, Y.K.T. Phan, T.H. Nguyen, D.V. Hoang, O.K.T. Le, T.B. Phan, V.C. Tran, Appl. Optics (2020). https://doi.org/10.1364/AO.395051

4. D. Aryanto, P. Marwoto, T. Sudiro, A.S. Wismogroho, Sugianto. Jour. Phys.: Conf. Series (2019). https://doi.org/10.1088/1742-6596/1191/1/012031

5. T. Miyata, H. Tokunaga, K. Watanabe, N. Ikenaga, T. Minami, Thin Sold. Films (2019). https://doi.org/10.1016/j.tsf.2020.137825

6. H.P. Pham, T.H.Y. Nguyen, A.H. Nguyen, N.T. Vo, T.G.L. Thuy, H.H. Nguyen, H.T.M. Hoa, Q.T. Tran, Jour. of Photo. and Photo-bio. A: Chemi. (2020) https://doi.org/10.1016/j.jphotochem.2019.112157

7. B. Sarma, D. Barman, B.K. Sarma, Appl. Surf. Science (2019). https://doi.org/10.1016/j.apsusc.2019.02.146

8. S. Sugianto, B. Astuti, N.A. Firmahaya, D. Aryanto, Isnaeni. Jour. Phys.: Conf. Series (2019). https://doi.org/10.1088/1742-6596/1387/1/012007

9. O.R. Alobaidi, P. Chelvanathan, B. Bais, K. Sopian, M.A. Alghoul, M. Akhtaruzzaman, N. Amin, Mater. Lett. (2021). https://doi.org/10.1016/j.matlet.2021.130551

10. M.S. Abdel-wahab, J. Elec, Material (2021). https://doi.org/10.1007/s11664-021-08963-z

11. M. Wang, F. Yang, S. Dai, Z. Cao, J. Su, S. Ding, P. Zhang, J. Light. Technology (2021). https://doi.org/10.1109/JLT.2021.3078146

12. H. Zhu, X. Niu, M. Wan, Y. Mai, Vacuum (2019). https://doi.org/10.1016/j.vacuum.2018.12.053

13. M. Laurenti, S. Porro, C.F. Pirri, C. Ricciardi, A. Chiolerio, Crit. Rev. S. S. Mat. Sci. (2017). https://doi.org/10.1080/10408436.2016.1192988

14. O. Zhao, Y. Ding, D. Cheng, J. Zhang, F. Hilt, N. Rolston, R.H. Dauskardt, Thin Solid Films (2021). https://doi.org/10.1016/j.tsf.2021.138708

15. S. Zhao, Y. Shen, Y. Xia, A. Pan, Z. Li, C. Carraro, R. Maboudian, J. All. Comp. (2021). https://doi.org/10.1016/j.jallcom.2021.160189

16. U.Chaitra, A.V.Muhammed Ali, M.G.Mahesha, A. Kompa, D. Kekuda, K. Mohan Rao, Superlatt. Micro. (2021) https://doi.org/10.1016/j.spmi.2021.106903

17. J.C.A. Queiroz, M. Naeem, J.B.A. Filho, M.S. Liborio, M.G.O. Queiroz, R.R.M. Sousa, E.B. Melo, M. Feitor, T.H.C. Costa, J. Mater. Resea. Tech. (2021). https://doi.org/10.1016/j.jmrt.2021.04.026

18. C. Bhoomanee, P. Ruankham, S. Choopun, D. Wongratanaphisan, Appl. Surf. Sci. (2019). https://doi.org/10.1016/j.apsusc.2018.04.082

19. K. Deva Arun Kumar, S. Valanarasu, S. Rex Rosario, Surf. Interf. Thin Films (2019) https://doi.org/10.1134/S1063782619040286

20. A. Catellani, A. Calzolari, Materials (2017). https://doi.org/10.3390/ma10040332

21. J.C.A. Queiroz, M. Naeem, J.B.A. Filho, M.S. Liborio, E.J.S. Costa, M. Feitor, R.R.M. Sousa, T.H.C. Costa, K.H. Khan, J. Elect, Materials (2021). https://doi.org/10.1007/s11664-021-08802-1

22. J.C.A. Queiroz, J.B.A. Filho, J.Q.M. Neto, I.O. Nascimento, I. A. Souza, M.G.O Queiroz, E.B. Melo, J.D.D. Melo, T.H.C. Costa, Proces. Applic. Ceramics (2020) https://doi.org/10.2298/PAC2002119Q

23. V.S.S. Sobrinho, J.Q.M. Neto, L.L.F. Lima, I.A. Souza, M.S. Librio, J.C.A. Queiroz, R.R.M. Sousa, E.O. Almeida, M.C. Feitor, T.H.C. Costa, Brazili. J. Phys. (2020) https://doi.org/10.1007/s13538-020-00794-3

24. J.C.A. Queiroz, J.B.A. Filho, M.C. Feitor, M.S. Librio, E.J.C. Santos, U.B. Souto, R.R.M. Sousa, T.H.C. Costa, Physi. Stat.

25. K. Sun, X. Tang, C. Yang, D. Jin, Ceram. Inter. (2018). https://doi.org/10.1016/j.ceramint.2018.07.207

26. L. Wen, B.B. Sahu, H.R. Kim, J.G. Han, Appl. Surf. Sci. (2019). https://doi.org/10.1016/j.apsusc.2018.11.250

27. C. Ma, X. Lu, B. Xu, F. Zhao, X. An, B. Li, L. Sun, J. Jiang, Y. Chen, J. Chu, J. Allo. Comp. (2019). https://doi.org/10.1016/j.jallcom.2018.09.056

28. A. Amini, M.S. Zakerhamidi, S. Khorram, Surf. Interf. (2021). https://doi.org/10.1016/j.surfin.2021.101028

29. V. Şenay, J. Mater. Sci. Mater. Electron. (2019). https://doi.org/10.1007/s10854-019-01329-6

30. A. Apaolaza, D. Richard, M.R. Tejerina, Proces. Applic. Ceramics (2020). https://doi.org/10.2298/PAC2004362A

31. A. Amini, M.S. Zakerhamidi, S. Khorram, Surf. Optik (2021). https://doi.org/10.1016/j.ijleo.2021.166772

32. Z. Du, X. Liu, Y. Zhang, Ceram. Inter. (2017). https://doi.org/10.1016/j.ceramint.2017.03.045

33. R. Nasser, J. Song, H. Elhouichet, Superl. Micro. (2021). https://doi.org/10.1016/j.spmi.2021.106908

34. I.L.P. Raj, S. Gobalakrishnan, P.K. Praseetha, N. Chidhambaram, S. Saravanakumar, V. Ganesh, S. AlFaify, H. Algarni, I.S. Yahia, Phys. Scrip. (2021). https://doi.org/10.1088/1402-4896/abfb22

35. B. Khalfallah, I. Riahi, F. Chaabouni, Opti. Quant. Elect. (2021). https://doi.org/10.1007/s11082-021-02861-8

36. M.S. Librio, G.B. Praxedes, L.L.F. Lima, I.G. Nascimento, R.R.M. Sousa, M. Naeem, T.H. Costa, S.M. Alves, Javed Iqbal, Surf. Coat. Techno. (2021) https://doi.org/10.1016/j.surfcoat.2019.125327

37. L.S. Birks, H. Friedman, J. Appl. Phys. (1946). https://doi.org/10.1063/1.1707771

38. J. Tauc, R. Grigorovici, A. Vancu, Phys. status solidi. (1966). https://doi.org/10.1002/pssb.19660150224

39. N. Chandra, V. Sharma, G.Y. Chung, D.K. Schroder, Solid. State. Electron. (2011). https://doi.org/10.1016/j.sse.2011.07.004

40. N. Fujimura, T. Nishihara, S. Goto, J. Xu, T. Ito, J. Cryst. Growth. (1993). https://doi.org/10.1016/0022-0248(93)90861-P

41. D.V. Hoang, N.H. Vu, N.T. Do, A.T.T. Pham, T.H. Nguyen, J. Kuo, T.B. Phan, V.C. Tran, J. Materiom. (2021). https://doi.org/10.1016/j.jmat.2021.04.011

42. U. Chaitra, A.V.M. Ali, M.G. Mahesha, A. Kompa, D. Kekuda, K.M. Rao, Super. Micro. (2021). https://doi.org/10.1016/j.spmi.2021.106903

43. F. Turkoglu, H. Koseoglu, S. Zeybek, M. Ozdemir, G. Aygun, L. Ozyuzer, J. Appl. Phys. (2018). https://doi.org/10.1063/1.5012883

44. M.S. Abdel-wahab, J. Elect. Mater. (2021). https://doi.org/10.1007/s11664-021-08963-z

45. H. Long, L. Bao, A.A. Habeeb, P. Lu, Opt. Quant. Elect. (2017). https://doi.org/10.1007/s11082-017-1170-9

46. I.L.P. Raj, S. Gobalakrishnan, P.K. Praseetha, N. Chidhambaram, S. Saravanakumar, V. Ganesh, S. AlFaify, H. Algarni, I.S. Yahia, Phys. Scrip. (2021). https://doi.org/10.1088/1402-4896/abfb22

47. S.S. Kumar, N. Chidhambaram, K.D.A. Kumar, R. Isaac, A.A. Abdeltawab, S.Z. Mohammady, M. Ubaidullah, S.F. Shaik, Semic. Scie. Technol. (2021) http://iopscience.iop.org/article/10.1088/1361-6641/abfadf

48. G.B. Lee, S.H. Song, M.W. Lee, Y.J. Kim, B.H. Choi, App. Surf. Scien. (2021). https://doi.org/10.1016/j.apsusc.2020.147731

49. S. Gopikishan, I. Banerjee, A. Pathak, S.K. Mahapatra, Radiat. Eff. Defects Solids (2017). https://doi.org/10.1080/10420150.2017.1359597

50. N. Srinatha, P. Raghu, H.M. Mahesh, A. Madhu, S. Hussain, S. Dam, S. Kumar, B. Angadi, Opt. Mater. (2021). https://doi.org/10.1016/j.optmat.2021.110872

Solid. Applic. Matr. Sci. (2020) https://doi.org/10.1002/pssa.202000167

51. S. Solaymani, A. Ghaderi, L. Dejam, Z. Garczyk, W. Sapota, S. Stach, V. Dalouji, C. Luna, S.M. Elahi, S.H. Elahi, Int. J. Hydrog. Energy (2017). https://doi.org/10.1016/j.ijhydene.2017.04.045

52. U. Chaitra, A.V. Muhammed Ali, M.G. Mahesha, A. Kompa, D. Kekuda, K.M. Rao, Spuerl. Micro. (2021) https://doi.org/10.1016/j.spmi.2021.106903

53. N. Ghobadi, M. Shivarand, E.G. Hatam, Opt. Quant. Elect. (2021). https://doi.org/10.1007/s11082-020-02687-w

54. C. Zhao, J. Liu, Y. Guo, Y. Pan, X. Hu, G. Weng, J. Tao, J. Jiang, S. Chen, P. Yang, J. Chu, J. Mater. Scien. Mater. Elect. (2021). https://doi.org/10.1007/s10854-021-05578-2

55. H. Sathish, K.N. Shaik, R.I. Kumar, A. Jafri, S.A. Reddy, Sattar. Ceram. Inter. (2021). https://doi.org/10.1016/j.ceramint.2021.02.037

56. L.G. Daza, I.V. Perez-Quintana, B. Cruz-Muoz, M. Herrera-Salvador, R. Castro-Rodrguez, Optik (2021) https://doi.org/10.1016/j.ijleo.2021.166561

57. L. Dejam, S. Mohammad Elahi, H. H. Nazari, H. Elahi, S. Solaymani, A. Ghaderi, J. Mater. Sci. Mater. Electron. (2016) https://doi.org/10.1007/s10854-015-3804-7

58. V.S. Rana, J.K. Rajput, T.K. Pathak, P.K. Pal, L.P. Purohit, Cryst. Resea. Tech. (2021). https://doi.org/10.1002/crat.202000144

59. F. Urbach, Physical Review, (1953) https://link.aps.org/doi/10.1103/PhysRev.92.1324

60. S. Jang, J.S. Jang, E. Jo, V.C. Karade, J. Kim, J.H. Moon, J.H. Kim, Kore. J. Mater. Resea. (2021) http://dx.doi.org/10.3740/MRSK.2021.31.3.150

61. S. Mandal, A. Basak, U.P. Singh, Mater. Proc. (2021). https://doi.org/10.1016/j.matpr.2020.05.029

62. X.N. Liu, J. Gao, J.H. Gong, W.X. Wang, S.C. Chen, M.J. Dai, S.S. Lin, Q. Shi, H. Sun, Ceram. Inter. (2021). https://doi.org/10.1016/j.ceramint.2020.10.153

63. B. Barman, S.K. Swami, V. Dutta, Mater. Sci. Semic. Proc. (2021). https://doi.org/10.1016/j.mssp.2021.105801

64. D. Mendil, F. Challali, T. Touam, V. Bockelee, S. Ouhenia, A. Souici, D. Djouadi, A. Chelouche, J. Alloys Comp. (2021). https://doi.org/10.1016/j.jallcom.2020.158470

65. H.T. Dao, H. Makino, Ceram. Inter (2021). https://doi.org/10.1016/j.ceramint.2020.11.160

66. K. Yujin, K. Sangmo, H. Jeongsoo, K.K. Hwan, Nanosci. Nanotech. (2021). https://doi.org/10.1166/jnn.2021.18928

67. L.P.G. Oliveira, R. Ramos, W.H. Rabelo, S.F. Durrant, J.R.R. Bortoleto, Mater. Resea. (2020) http://dx.doi.org/10.1590/1980-5373-mr-2019-0643

68. X. Zhang, R. Zhu, J. Phys. Conf. Series (2020). https://doi.org/10.1088/1742-6596/1549/4/042006

69. N. Vasile, S. Iftimie, T. Acsente, C. Locovei, A.I. Calugar, A. Radu, L. Ion, V. Antohe, D. Manica, O. Toma, G. Dinescu, S. Antohe, Mater. Res. Exp. (2020). https://doi.org/10.1088/2053-1591/ab688d

70. Y.H. Sun, H.L. Wang, J. Chen, L. Fang, L. Wang, Trans. Nonfer. Met. Soc. China (2016). https://doi.org/10.1016/S1003-6326(16)64275-9

71. F. Challali, D. Mendil, T. Touam, T. Chauveau, V. Bockelee, A.G. Sanchez, A. Chelouche, M.P. Besland, Mater. Sci. Semicond. Process. (2020). https://doi.org/10.1016/j.mssp.2020.105217

Publisher's Note Springer Nature remains neutral with regard to jurisdictional claims in published maps and institutional affiliations.